ELSEVIER

Physica D 76 (1994) 70–84

PHYSICA D

Chaotic advection in a two-dimensional flow: Lévy flights and anomalous diffusion

T.H. Solomon[1], Eric R. Weeks[2], Harry L. Swinney[3]

Center for Nonlinear Dynamics and Department of Physics, University of Texas at Austin, Austin, TX 78712, USA

Abstract

Long-term particle tracking is used to study chaotic transport experimentally in laminar, chaotic, and turbulent flows in an annular tank that rotates sufficiently rapidly to insure two-dimensionality of the flow. For the laminar and chaotic velocity fields, the flow consists of a chain of vortices sandwiched between unbounded jets. In these flow regimes, tracer particles stick for long times to remnants of invariant surfaces around the vortices, then make long excursions ("flights") in the jet regions. The probability distributions for the flight time durations exhibit power-law rather than exponential decays, indicating that the particle trajectories are described mathematically as Lévy flights (i.e. the trajectories have infinite mean square displacement per flight). Sticking time probability distributions are also characterized by power laws, as found in previous numerical studies. The mixing of an ensemble of tracer particles is *superdiffusive*: the variance of the displacement grows with time as t^γ with $1 < \gamma < 2$. The dependence of the diffusion exponent γ and the scaling of the probability distributions are investigated for periodic and chaotic flow regimes, and the results are found to be consistent with theoretical predictions relating Lévy flights and anomalous diffusion. For a turbulent flow, the Lévy flight description no longer applies, and mixing no longer appears superdiffusive.

1. Introduction

The mixing of passive impurities in fluid flows depends critically on the structure and time dependence of the velocity field. In the absence of a flow, Brownian motion of individual tracer particles results in molecular diffusion, characterized by the variance of the displacement of a particle distribution σ^2 which grows linearly with time: $\sigma^2(t) \sim t^\gamma$, with $\gamma = 1$. If the fluid is moving, advection of tracer particles by the flow results in significant enhancements in the transport rates. For many flows of interest, the variance of a distribution grows as a power law with time. If $\gamma = 1$, the enhanced mixing is termed "normal" diffusion, while mixing with $\gamma \neq 1$ is termed "anomalous" diffusion [1–3].

If the tracer trajectories are dominated by sticking regions where tracers are detained for long periods of time, anomalous diffusion with $\gamma < 1$ (subdiffusion) results [4]. On the other hand, if there are jet regions in the flow, tracer particles may travel long distances between sticking events. If these excursions are described by length and time probability distribution functions

[1] Current address: Department of Physics, Bucknell University, Lewisburg, Pennsylvania 17837; E-mail: tsolomon@bucknell.edu

[2] E-mail: weeks@chaos.utexas.edu

[3] E-mail: swinney@chaos.utexas.edu

SSDI 0167-2789(94)00041-N

that have power law (rather than exponential) tails, then superdiffusion ($1 < \gamma < 2$) may result [1–3, 5–9]. Long excursions with power law distributions – Lévy flights – have the interesting property that the mean square displacement per step diverges [1,2]. (This does not, however, mean that the variance of the displacement of an ensemble of particles is infinite for Lévy flights.) Recent theoretical studies of *chaotic advection* (or "Lagrangian chaos") of tracers in fluid flows have demonstrated mechanisms by which Lévy flights may occur in real mixing problems [3]. To date, however, there have been no direct observations of Lévy motion in fluid flows.

This article presents experimental measurements of Lévy flights and superdiffusive transport in a two-dimensional flow in a rotating annulus [10]. The flow consists of a chain of vortices sandwiched between jet regions (Fig. 1) [11–13]. Long-term tracking of large numbers of particles in the flow [14] makes possible quantitative measurements of the variance of the displacement and the sticking and flight time probability distribution functions. Studies are made in four different flow regimes: time-independent, time-periodic, chaotic, and turbulent. We explore the dependence of the scaling of the variance and the flight and sticking statistics on the time dependence of the flow.

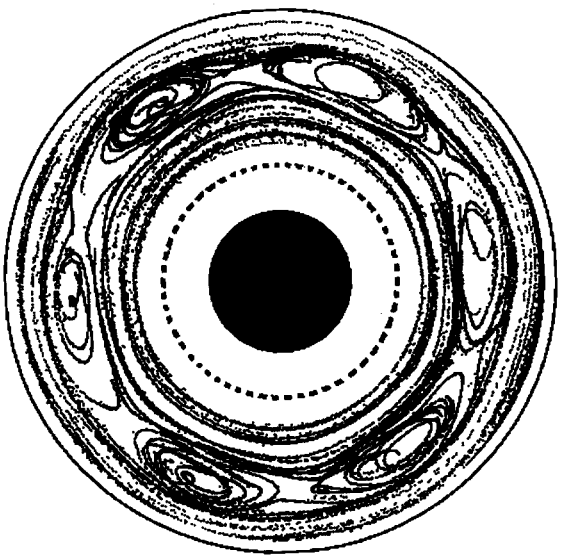

Fig. 1. Streaks formed by 90 s long trajectories of about 40 particles reveal the presence of six vortices sandwiched between two azimuthal jets, as viewed in a reference frame co-rotating with the vortex chain. The vortex chain rotates with a frequency 0.01429 Hz slower than the 1.5 Hz rotation frequency of the annulus. The dashed circle represents the outer radius of the inserted Plexiglas barrier.

2. Background

2.1. Hamiltonian formalism and Lévy flights

Transport in a two-dimensional flow can be analyzed from a Hamiltonian perspective [15]. Given a stream function $\psi(x, y, t)$ the equations describing particle motion in the flow are given by

$$\frac{dx}{dt} = -\frac{\partial \psi}{\partial y}, \quad \frac{dy}{dt} = \frac{\partial \psi}{\partial x}, \tag{1}$$

which are Hamilton's equations of motion with ψ as the Hamiltonian and x and y as the conjugate coordinates. The path of a passive tracer in a two-dimensional flow is, therefore, the phase-space trajectory of a Hamiltonian system. If ψ is time-independent, the equations of motion are fully integrable and trajectories follow the streamlines. In time-independent cellular flows, for example, particles within a vortex (a cell) ideally remain trapped indefinitely; see Fig. 2a.

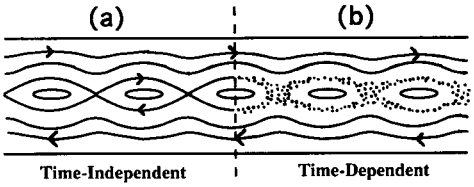

Fig. 2. (a) Phase space portrait for an ideal time-independent (integrable) system; all trajectories are closed curves (b) Poincaré section for a time-dependent (non-integrable) system; some trajectories lie on closed curves (KAM tori), but there are large regions (the chaotic sea) with chaotic trajectories. For the fluid flow in the annulus, the phase space is *real* space.

In reality [4,16], molecular diffusion allows tracers eventually to escape from the vortices, although the time scale for the escape can be quite long compared to the characteristic times for the dynamics (e.g. vortex turnover time). The combination of advection and molecular diffusion results in transport that is typically enhanced with $\gamma = 1$ for long times, although subdiffusion ($\gamma < 1$) is possible for times shorter than diffusive mixing times [4].

If the flow is time-dependent, the Hamiltonian phase space (real space for fluid mixing) can be divided into ordered and disordered regions; see Fig. 2b. Tracer particles in the disordered regions follow chaotic trajectories. This behavior is termed Lagrangian chaos or chaotic advection [15,17]. The resultant particle trajectories are often far more complicated than might be expected for a laminar flow. In the absence of molecular diffusion, the curves (invariant surfaces) dividing the ordered and disordered regions act as impenetrable barriers that tracer particles cannot cross.

The motion of tracer particles within the disordered regions is affected by the invariant surfaces (KAM tori) or their remnants (Cantori). Particles that pass close to an invariant surface remain in the vicinity of that surface for a long (but finite) time [18–19]. The persistence of trajectories near closed surfaces results in long-time *sticking* of particles. Similarly, if a flow contains jet regions and Cantori, long-range and long-time excursions called *flights* are possible. (Some authors define a flight as an instantaneous jump, i.e. motion with infinite velocity [3], while finite-velocity excursions in this terminology are called walks; we use the term flight for long excursions even though the velocity is finite.) Theoretical studies of sticking in Hamiltonian models [18–25] have predicted sticking times with probability distribution functions (PDFs) that are power laws: $P_S(t) \sim t^{-\nu}$. Similarly, power law relations are expected for flights in two-dimensional flows: $P_F(t) \sim t^{-\mu}$ [3,5–7,19].

Long-time flights provide a conceptual link between chaotic advection and anomalous diffusion. Trajectories with power law flight PDFs (with decay exponent $\mu < 3$) are called *Lévy flights* [2]: random walks with infinite mean square displacement per flight. Several theoretical studies predict that power law PDFs can give rise to superdiffusive transport. In models by Geisel et al. [5], Klafter et al. [6] and Wang [7], the scaling of $\sigma^2(t)$ is dominated by the flight-time statistics, and the relation between the variance and flight exponents (for flights with a constant velocity) is

$$\gamma = 4 - \mu \,. \tag{2}$$

In a Hamiltonian model of Zaslavsky [26] both the flight and sticking PDFs are important in determining the scaling of the variance:

$$\gamma = 2\nu/(\mu - 1) \,. \tag{3}$$

Neither (2) nor (3) has been tested experimentally.

2.2. Previous experiments

Measurements of transport enhancement due to chaotic advection have been made for time-periodic convection [27]; in those flows there were no jet regions so there were no flights, and the diffusion was normal with $\gamma = 1$. Studies of transport in turbulent surface waves [28] and oceanic flow [29,30] yielded evidence of super-diffusion and fractal scaling of individual trajectories, but the mechanisms responsible for the observed behavior were unclear. Furthermore, too few trajectories were observed to characterize accurately the flight-time probability distribution functions.

The only previous discussion of Lévy flights in an experimental system examined anomalous self-diffusion in polymer-like breakable micelles, fitting experimental measurements to a model that assumed Lévy behavior [31]. Flight and sticking-time probability distribution functions have not been determined in any experiments.

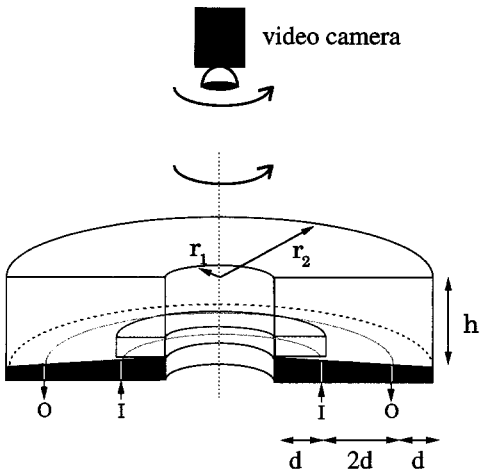

Fig. 3. Schematic diagram of the rotating annulus. Flow is produced by pumping fluid into the annulus through an inner ring of holes (marked I) and out of the tank through an outer ring of holes (marked O). The motion of particles in the flow is observed with a rotating video camera mounted coaxially above the annulus.

3. Experiments

The experiments are conducted in an annular tank (Fig. 3) that rotates rigidly at a rate of 1.5 Hz (9.425 rad/s). The working volume has an inner radius $r_1 = 10.8$ cm and an outer radius $r_2 = 43.2$ cm. The lid is flat and the bottom surface is slightly conical, with height $h = 17.1$ (20.3) cm at the inner (outer) radius; see discussion in [11–13]. The conical bottom models the effect of planetary curvature on atmospheric and oceanic flows; this effect is not of importance to the transport studies presented here [11]. A 6 cm tall Plexiglas annulus with inner (outer) radius of 10.8 (19.4) cm is inserted into the tank to act as a barrier; this barrier, by the Taylor–Proudman theorem, divides the flow into inner and outer regions. The annulus is filled to the top with a mixture of 38% glycerol (by weight) in water (kinematic viscosity $\nu = 0.03\,\mathrm{cm}^2/\mathrm{s}$), except in the experiments on turbulent flow where water (kinematic viscosity $\nu = 0.009\,\mathrm{cm}^2/\mathrm{s}$) was used to increase the Reynolds number.

A flow is produced in the annulus by pumping the fluid into and out of the tank through 0.26 cm diameter holes in the bottom. The holes are arranged in two concentric rings of 120 holes at radii 18.9 and 35.1 cm. In all experiments the flow rate of the forcing flow is $45\,\mathrm{cm}^3/\mathrm{s}$. Two forcing techniques are used:

(1) *Radial forcing.* In this configuration the inner (outer) ring of holes acts as a source (sink) through which fluid is pumped into (from) the tank. The resulting radial forcing flow couples with the Coriolis effect to produce a strong azimuthal jet that rotates (relative to the tank) in the direction opposite the rotation of the tank. Jet velocities are typically two orders of magnitude greater than those of the forcing flow.

(2) *Azimuthally alternating forcing.* In this configuration only the outer ring holes are used. The ring is divided into six 60° sectors, alternating between sources and sinks. The resulting flow consists of vortices of both signs, and there is no persistent jet.

For both configurations, the rapid rotation of the system results in a flow that is predominantly two-dimensional [13], as expected by the Taylor–Proudman theorem [32].

The temperature of the system is monitored with a thermistor probe in the fluid lines below the tank, and is maintained at $25.5 \pm 0.5\,^\circ\mathrm{C}$. Spatial non-uniformities in the temperature of the tank are minimized by pumping fluid at $45\,\mathrm{cm}^3/\mathrm{s}$ through the inner and outer holes for at least 3/4 hour before each experimental run. This technique minimizes convective flows due to density variations.

Velocity measurements are made with hot-film probes mounted in the lid [13].

4. Dynamics of the velocity field

The radial forcing configuration was used for all experiments except those on turbulent flow,

which used the azimuthally alternating forcing configuration. With the radial forcing the flow is a counter-rotating azimuthal jet between the source and sink rings. The jet is bounded by sharp velocity gradients above the edge of the Plexiglas barrier and above the outer ring of holes. At a sufficient flow rate ($\sim 10\,\mathrm{cm}^3/\mathrm{s}$), the outer shear layer becomes unstable to the formation of a chain of vortices that precesses around the tank [13]. The inner shear layer is a Stewartson boundary layer, so it does not become unstable to the formation of a vortex chain (this is the reason for the insertion of the Plexiglas barrier). The measurements reported in this paper, except those on turbulent flow, were made on chains of six vortices. From the perspective of a reference frame moving with the vortices (Fig. 1), the chain is sandwiched between two azimuthal jets.

Experiments are done on four different types of velocity fields:

– *Time-independent flow:* This flow with a circular chain of six vortices is time-periodic in the reference frame of the tank but is time-independent in a reference frame that co-rotates with the vortex chain; see Fig. 4a. Ideally, particle trajectories in this flow follow the streamlines, and there is no chaotic mixing.

– *Time-periodic flow:* In this regime, the velocity field is simply periodic in the co-rotating frame of the vortex chain but is doubly periodic in other reference frames, except for the reference frame of the tank. This flow is produced using radial forcing with a non-axisymmetric perturbation: the forcing flow through one 60° sector of source and sink holes is restricted to less than half that for the rest of the forcing holes. Thus the size of each vortex diminishes as the vortex moves through the restricted region. The period of the perturbation is the time for a vortex to precess around the annulus (70.0 s). In the reference frame of the tank (Fig. 4b), the time dependence is similar to the time-independent flow case, since the perturbation is stationary in the tank's reference frame. In this regime, chaotic particle trajectories are common, despite the fact that the flow is laminar.

– *Chaotic flow:* A chaotic velocity field is obtained with one 60° sector of source and sink holes closed completely; see Fig. 4c. There are still well-defined vortices in the flow, but the number of vortices alternates between five and six over long periods of time.

– *Turbulent flow:* A turbulent flow cannot be achieved with our low flow rate pump for the radial forcing configuration, but a turbulent flow is obtainable with the low pump rate for another flow configuration, one with azimuthally alternating forcing. The turbulence is enhanced by using water as the working fluid to increase the Reynolds number. The resulting turbulent flow has no persistent vortices. The velocity power spectrum consists of broadband noise and no dominant spectral components; see Fig. 4d.

5. Particle-tracking and analysis techniques

5.1. Tracer particles

The particles are made from fluorescent crayons (Crayola® brand: atomic tangerine, sunglow, unmellow yellow and laser lemon) that are melted together, mixed with concrete powder to increase the density, then chopped and sieved to produce 1–2 mm cubical particles. The particles are suspended in a sample of the working fluid that has been heated to drive out dissolved air. Particles used in the experiment are those that remain suspended in the sample for at least four minutes. This method produces particles that will remain suspended in the flow for hours, even with the tank spinning at 1.5 Hz where centrifugal accelerations are up to four times that of gravity.

Stokes drag can cause particle trajectories to deviate from those for ideal passive particles, even if the particles are neutrally buoyant. This effect is quantified by the dimensionless Stokes

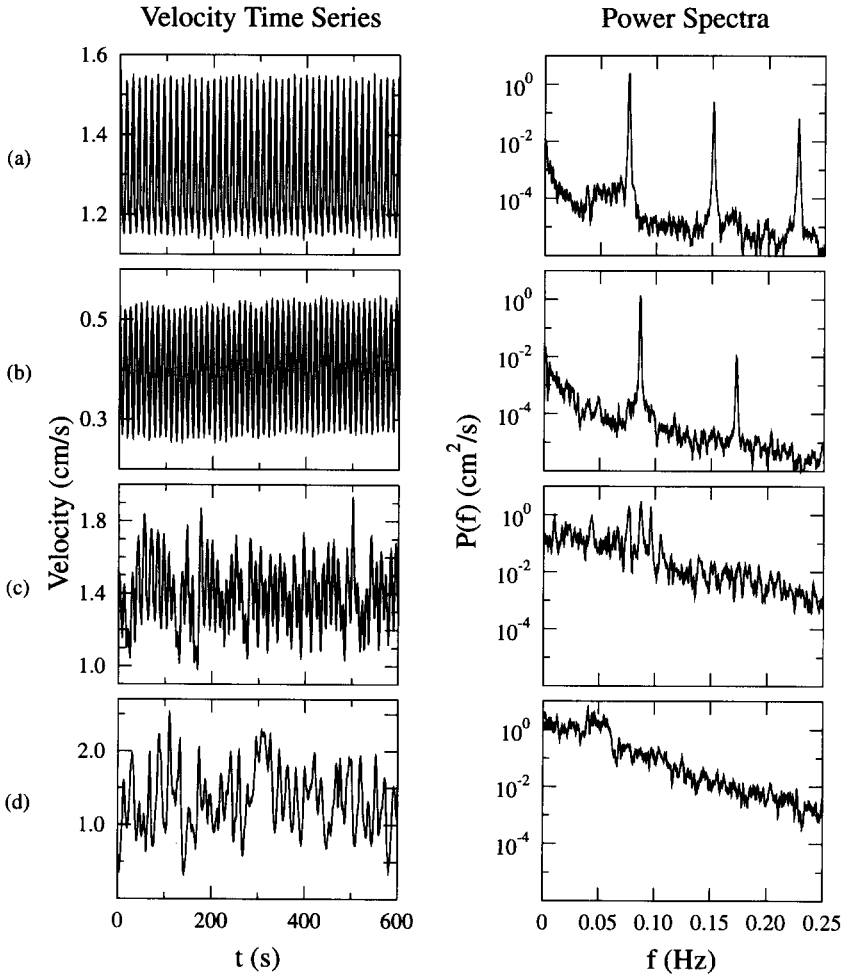

Fig. 4. Velocity time series and power spectral density $P(f)$ obtained from measurements of the azimuthal velocity component at $r = 35.1$ cm: (a) A flow which is periodic in the tank frame and time-independent in the reference frame co-rotating with the six vortices – see Fig. 1; (b) time-periodic flow; (c) chaotic flow; (d) turbulent flow. Because the time series are taken in the tank frame of reference, and the perturbation of the flow in (b) is fixed in this tank frame, the power spectrum in (b) is periodic in both the tank frame and in the frame co-rotating with the vortex chain.

number, which is given by $S \cong Ud^2/18\nu L$ for a neutrally buoyant particle, where d is the particle diameter, ν is the kinematic viscosity of the fluid, and U and L are the characteristic velocity and length scales of the flow [33]. Drag effects are negligible if $S \ll 1$. For a typical velocity scale (1 cm/s) and length scale (10 cm), we have $S \cong 0.002$, insuring that the particles are sufficiently passive on these scales. For very small structures in the flow, the particles will not follow precisely the velocity field. Other effects that can cause particles to deviate from the ideal trajectories (e.g. Bassett and "added mass" effects [33]) are negligible in these experiments.

5.2. *Image acquisition and real-time analysis*

Particles in the flow are illuminated in a 6 cm tall horizontal section near the midheight of the annulus. Care is taken not to illuminate any tracers in the vicinity of either the upper or lower Ekman layers, which are only 0.6 mm

thick [11]. Because of the two-dimensionality of the flow [13], tracer particles remain in the illuminated regions for long times, typically 30 min, but Ekman pumping [11] results in slow vertical drifts that ultimately limit the tracking times that can be achieved.

The illuminated particles are imaged with a charge-coupled device video camera (Sanyo VDC 3800) whose rotation rate can be tuned to match the rotation rate of the reference frame of the propagating vortex chain; see Fig. 3. The video signal is partially processed [14] in real time with a Matrox IM-640 image processor installed in a PC-compatible workstation (Austin Computer Systems 486/33E). For each frame, the image processor subtracts a reference image and identifies bright pixels (i.e., those associated with particles in the flow) whose coordinates (encoded as 3-byte words) are transferred to the host PC and stored to disk. Up to 15 images/s (30 images/s without background subtraction) can be processed in real time with this approach, although frame rates of 10 images/s are used in the present experiments. In a typical image about 40 illuminated particles are visible, each represented by a cluster of approximately 10 pixels. The processing therefore results in a reduction of the data rate to 10–15 kbytes/s, small enough to enable real-time storage of the data with conventional hard disks. The data reduction also allows experimental runs to continue for long durations without filling up the disk: runs of 7 hours, for example, generate data files containing 300–400 Mbytes of pixel coordinates, far smaller files than would be generated by 7 hours of unprocessed images (67 Gbytes at 10 frames/s).

5.3. *Particle-tracking and transport analysis*

After an experimental run is completed, the stored pixel coordinates are analyzed to identify contiguous clusters of pixels corresponding to a tracer particle and to extract the individual trajectories. (See [14] for more details.) For a typical run of 4 hours with about 30 tracers visible at any given time, there are typically 5–10 trajectories with duration greater than 20 minutes, 30 with 10–20 minutes duration, and several hundred with 2–10 minutes duration. Statistics for the longer times are improved by repeating the experiments with the same control parameters.

The transport is analyzed as a one-dimensional process in the azimuthal direction θ. The variance is calculated by the relations

$$\sigma^2(t) = \langle (\Delta\theta(t,\tau) - \langle \Delta\theta(t,\tau) \rangle)^2 \rangle ,$$
$$\Delta\theta(t,\tau) = \theta(\tau + t) - \theta(\tau) , \qquad (4)$$

where the ensemble average is over τ for individual trajectories and over the different trajectories in the run. (τ serves as an offset, in integral multiples of the typical vortex turnover time of 20 s, that treats different sections of each trajectory as additional trajectories with new initial locations.) This procedure treats each tracer as though starting from the same angle at the same time. This method is accurate for times greater than typical vortex turnover times (20 s) but results in a variance that grows as t^2 for short times. Only those trajectories that display both sticking and flight events are used in the calculation of the variance, and the first sticking and last flight events are removed to avoid any biasing. Different analysis techniques were examined to insure that the results presented in this paper are not strongly dependent on the biasing effects.

Sticking and flight time probability distribution functions (PDFs) are determined from local extrema of $\theta(t)$; see e.g. Fig. 7. A flight is identified by an angular deviation $\Delta\theta > \pi/3$ (angular width of a single vortex) between successive extrema, and the sticking events are the intervals between flights. The PDFs are are normalized histograms of these events. The PDFs are adjusted to correct for biases toward shorter sticking/flight times, due to the finite duration of the measured trajectories. The adjustment is determined by generating long, artifi-

cial trajectories numerically with known, ideal, power-law sticking and flight time distributions. These long trajectories are then chopped randomly into smaller sections with a distribution of durations comparable to those in the experiment. PDFs determined from these chopped trajectories are also biased toward smaller times. The adjustment is determined by comparing the PDFs from the chopped trajectories to the ideal PDFs (both from numerical data); the exponents characterizing the PDFs for the chopped time series are about 0.3 larger than for the original long time series.

6. Results

6.1. Time-independent flow: no chaotic mixing

Ideally, particle trajectories in a time-independent flow fall on closed streamlines and there is no chaotic advection. While molecular diffusion of the tracer particles is completely negligible on the time scale of the experiments, slight imperfections due to noise (mainly from a small non-uniformity in temperature), Ekman pumping, and finite-size particle effects can have a noticeable effect on the trajectories. Such imperfections are inevitable in an experiment, even when Fourier spectra indicate that the velocity field is time-independent, as is the case for the flow in Fig. 5. The imperfections allow tracers to wander between neighboring streamlines, apparently filling the interior of a vortex; see Fig. 5. The imperfections occasionally lead to the escape of a tracer particle near a separatrix, but we find that in practice tracers remain trapped for long periods of time. Trapping times of 800 s – approximately 40 vortex turnover times – are common; see Fig. 5a. Similarly, tracers that start in a jet remain in the jet for long times; see Fig. 5b.

The azimuthal coordinate $\theta(t)$ for a particle in a vortex oscillates about a constant value, while for a particle in a jet $\theta(t)$ grows linearly with time, as shown in Fig. 5c. In the absence of noise, the variance of a distribution of particles grows as t^2 (ballistic separation) [34].

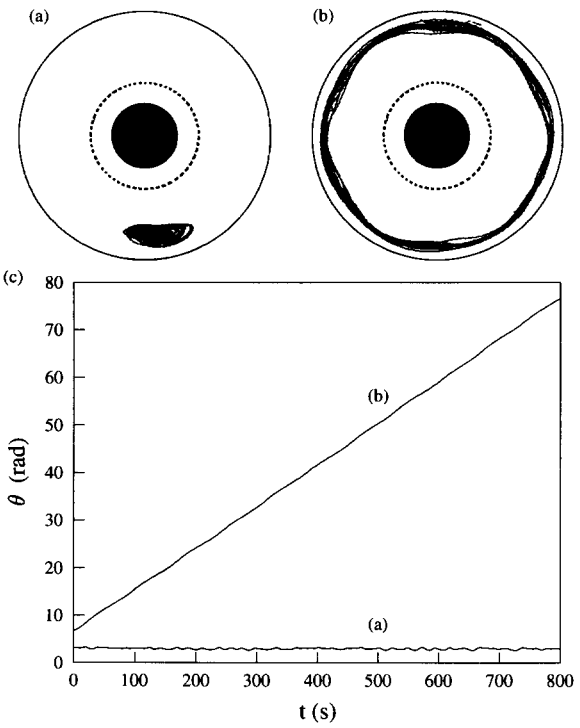

Fig. 5. (a) and (b) Tracer particle trajectories in the time-independent flow, viewed in a reference frame co-rotating with the vortex chain. (c) The azimuthal displacement as a function of time for the particles in (a) and (b); the starting angle $\theta(t=0)$ is arbitrary. The inner and outer circles represent the annulus boundaries, and the dashed circle denotes the outer edge of the Plexiglas barrier.

6.2. Time-periodic flow: Lévy flights and superdiffusion

Particle trajectories in the time-periodic flow are typically chaotic; see Fig. 6. Instead of being trapped indefinitely, particles have sticking events interspersed with flights in the jet regions. This intermittent sticking/flight behavior is apparent in plots of $\theta(t)$, as shown in Fig. 7. The observed sticking times and flight times range from ~10 s (one-half a vortex turnover time) to ~600 s. The slopes of the flight segments are approximately constant, indicating that the

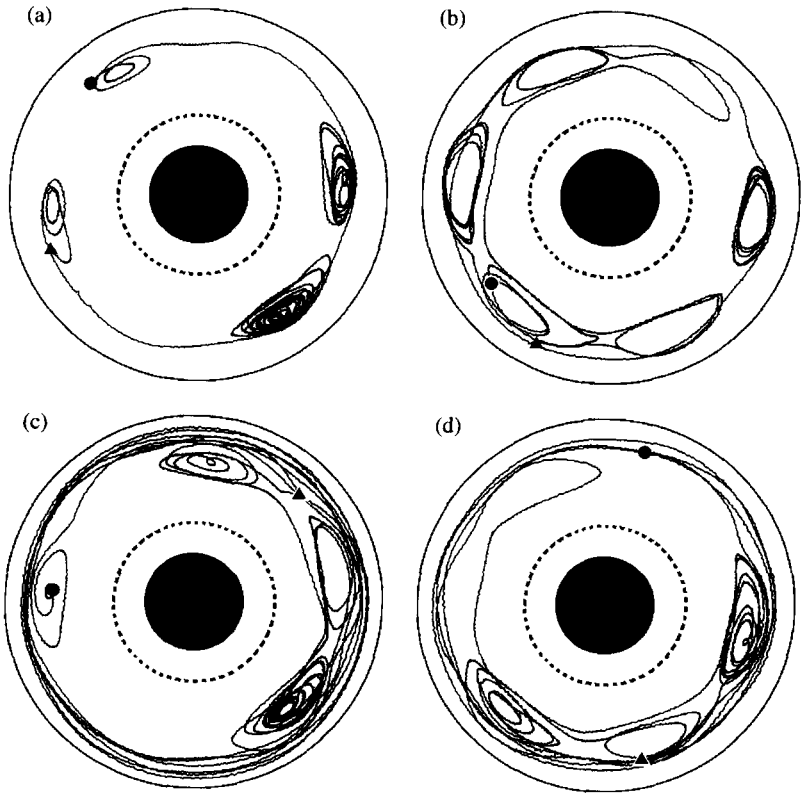

Fig. 6. Chaotic particle trajectories in a time-periodic flow. Long sticking events can be seen in each case, and flights of length greater than one rotation about the annulus can be seen in (c), (d). Hyperbolic fixed points, near which the particle motion is particularly sensitive to transitions between flights and sticking events, are evident in all the trajectories. The particle motion is viewed from a reference frame that is co-rotating with the vortex chain, and the beginning of each trajectory is marked by a circle, the end by a triangle.

azimuthal velocity, $\omega = d\theta/dt$, remains steady during the flights, except when the tracer passes near a hyperbolic point, where both ω and the radial component of velocity can decrease nearly to zero.

Fig. 8 is a scatter plot of the azimuthal displacement $\Delta\theta(t)$ of a distribution of tracers in the time-periodic case. High concentrations along the horizontal axis and along diagonals illustrate the importance of sticking events and flights, respectively, on the transport phenomena. There is an asymmetry between positive and negative displacements, due to a higher probability for corotating than for counter-rotating flights. This asymmetry in the flights is likely due to the curvature of the system, which results in longer and more curved separatrices outside the vortex chain than inside (see Fig. 6) and a larger exchange rate between the vortices and the outer jet [35].

Approximately 40 hours of data from six experimental runs (each 6–7 hours duration) are combined to determine the variance and the statistical properties. The variance $\sigma^2(t)$ is shown in Fig. 9. The slope γ of the log–log plot (see inset) drops from the expected value of 2 at short times (see Section 5.3) and forms a plateau at $\gamma = 1.65 \pm 0.15$ for times $t > 10$ s, indicating superdiffusive mixing. We are unable to characterize accurately the width of the plateau, since the data become unreliable for $t \gtrsim 1000$ s (due to poor statistics at these times).

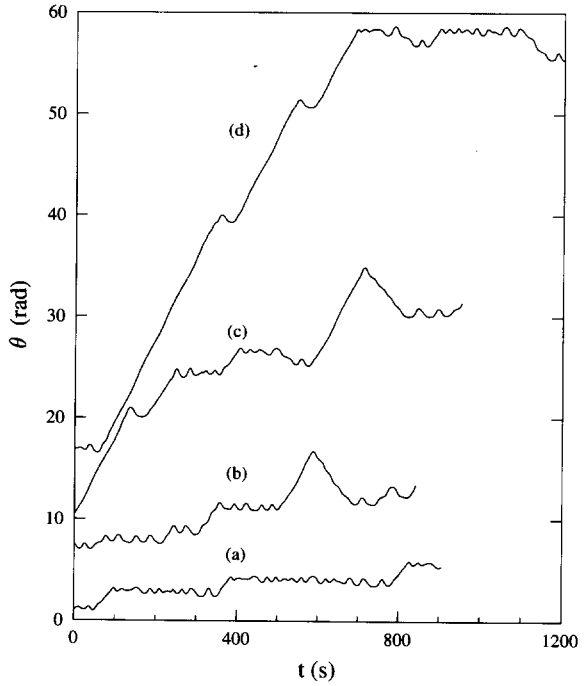

Fig. 7. Azimuthal displacement $\theta(t)$ as a function of time for the particle trajectories in Fig. 6. The oscillations of the tracer particle trajectories correspond to motion around a vortex, and the diagonal lines correspond to flights. The starting angle $\theta(t=0)$ is arbitrary.

The probability distribution function (PDF) of sticking times, $P_S(t)$, shown in Fig. 10a, exhibits a power law decay (for $t < 300$ s) with an exponent $\nu = 1.6 \pm 0.3$. (A semi-log plot of the data has a definite upward curvature for $t < 300$ s, indicating that the PDF is not exponential.) There is a slight drop-off in P_S from power law scaling for $t > 300$ s, indicating a possible transition to exponential decay at large times. This drop-off may occur because our 1–2 mm diameter tracer particles cannot probe small structures [33], such as higher order island chains. On these length scales, the Stokes number (Section 5.1) can approach unity, and drag effects on the particles can no longer be neglected.

The flight time PDF also exhibits power law scaling: $P_F(t) \sim t^{-\mu}$, with $\mu = 2.3 \pm 0.2$ (see Fig. 10b), indicating that the trajectories can be characterized mathematically as Lévy flights.

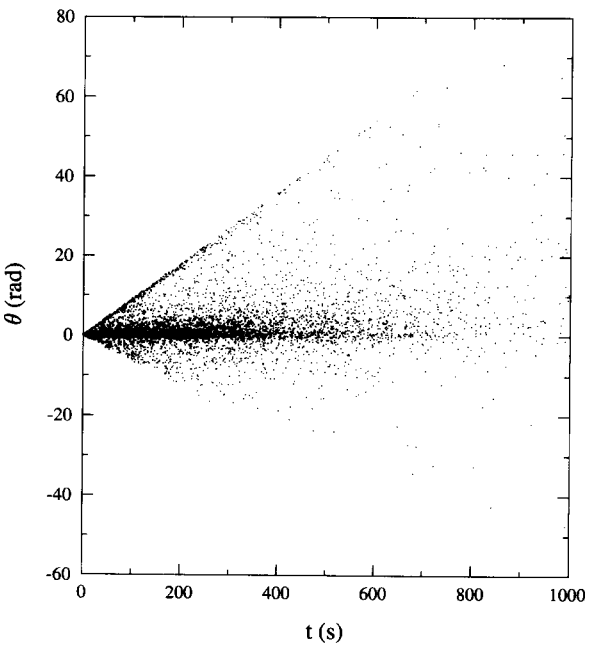

Fig. 8. Scatter plot showing the azimuthal positions of an ensemble of particles at discrete times for the time-periodic flow (where $\theta(t=0) = 0$ for all particles).

Data from both co- and counter-rotating flights have been included in the calculation of P_F. Separate plots of the PDF for co- and counter-rotating flights show power law scaling with the same decay exponent μ, within experimental uncertainty.

The flight *length* PDF is also described by a

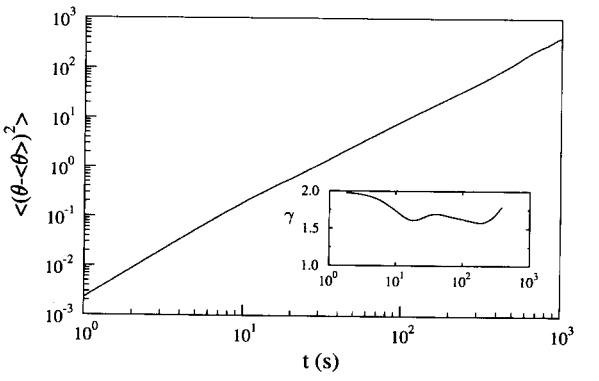

Fig. 9. Variance of the azimuthal displacement of about 3000 tracer particle trajectories in a time-periodic flow. The slope, shown in the inset, has a plateau that yields the exponent for the power-law growth, $\gamma = 1.65 \pm 0.15$ (*superdiffusion*).

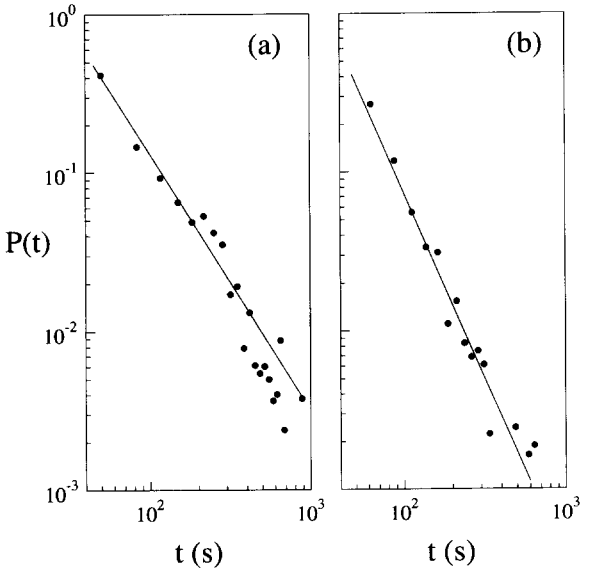

Fig. 10. (a) Sticking-time and (b) flight-time probability distribution functions for particles in the time-periodic flow. The distribution functions are described by power laws with decay exponents $\nu = 1.6 \pm 0.3$ and $\mu = 2.3 \pm 0.2$, respectively.

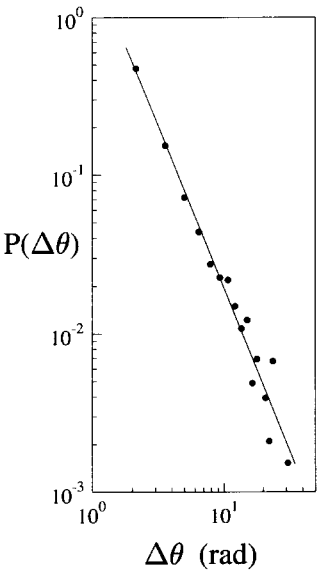

Fig. 11. Flight length probability distribution in the time-periodic flow, showing a power law decay with exponent $\eta = 2.05 \pm 0.30$.

power law: $P_L \sim \theta^{-\eta}$, with $\eta = 2.05 \pm 0.30$; see Fig. 11. The exponents for the flight length and time PDFs are the same (within experimental uncertainty) because the flight lengths $\Delta\theta$ and times Δt are linearly related, as shown in Fig. 12. There is a slight curvature for small Δt, caused by decreases in the azimuthal velocity when tracers pass near hyperbolic points. Since flights begin and end with tracers near hyperbolic points, this effect is most prominent for short flights.

6.3. Chaotic flow

One 7-hour experimental run was performed in the chaotic regime. Plots of $\theta(t)$ for particles in the chaotic velocity field still reveal well-defined sticking events and flights, as illustrated in Fig. 13. A scatter plot of $\Delta\theta(t)$ for an ensemble of particles (Fig. 14) is similar to that for the time-periodic case (Fig. 8), although the flights and sticking events do not dominate the transport as much (i.e. the concentrations along the horizontal axis and diagonals are not as high). The slope γ does not form a plateau at 1.65 (see Fig. 15); rather, it continues to drop, forming what might be the beginning of a plateau $\gamma = 1.55 \pm 0.25$ for $t > 80$ s. We do not have enough long trajectories to extend the graph beyond $t \approx 500$ s, so it cannot be determined if the asymptotic behavior is superdiffusive.

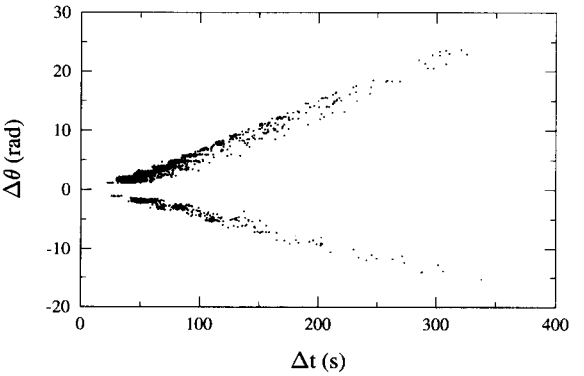

Fig. 12. Flight length $\Delta\theta$ versus flight duration Δt. The approximately linear relationship shows that flights have roughly constant velocity. The horizontal bands differ in spacing by $\pi/3$, which is the angular spacing between vortices.

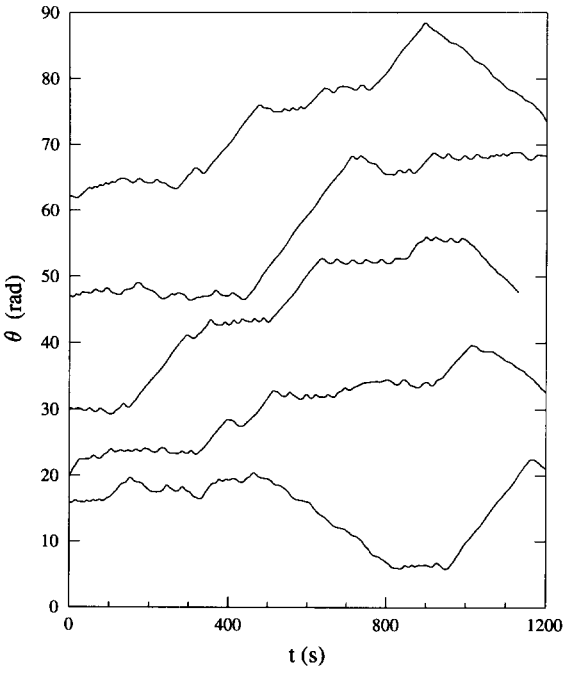

Fig. 13. The azimuthal displacement $\theta(t)$ for five typical trajectories in the chaotic flow, showing the presence of flights and sticking events. The starting angle $\theta(t=0)$ is arbitrary.

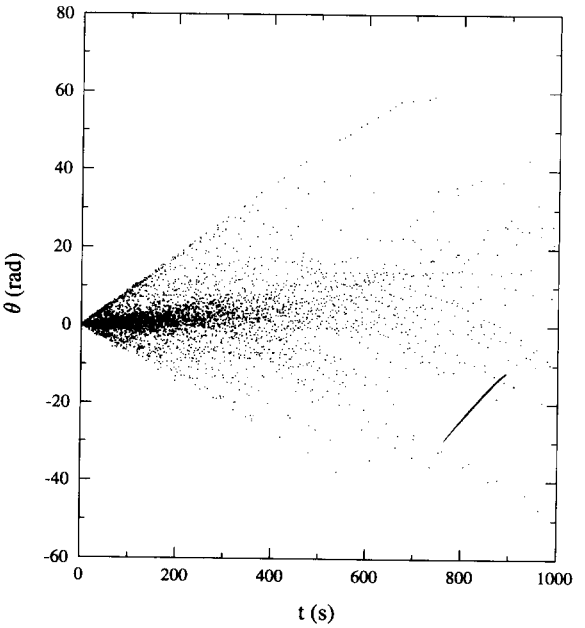

Fig. 14. Scatter plot showing the azimuthal positions of an ensemble of particles at discrete times for the chaotic flow (where $\theta(t=0)=0$ for all particles).

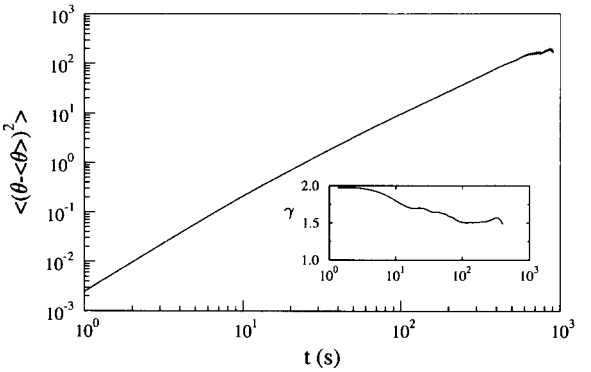

Fig. 15. Variance of the azimuthal displacement of about 600 tracer particle trajectories in a chaotic flow. The slope, shown in the inset, has a plateau (for $t>80$ s) that yields the exponent for the power law growth, $\gamma = 1.55 \pm 0.25$ (super-diffusion).

As was the case for the time-periodic flows, the sticking and flight time PDFs can both be characterized by power law relations, as shown in Fig. 16. The added flow complexity, however, reduces the typical sticking and flight times, resulting in larger decay exponents: $\nu = 2.1 \pm 0.3$ and $\mu = 2.6 \pm 0.3$ for sticking and flight time distributions, respectively.

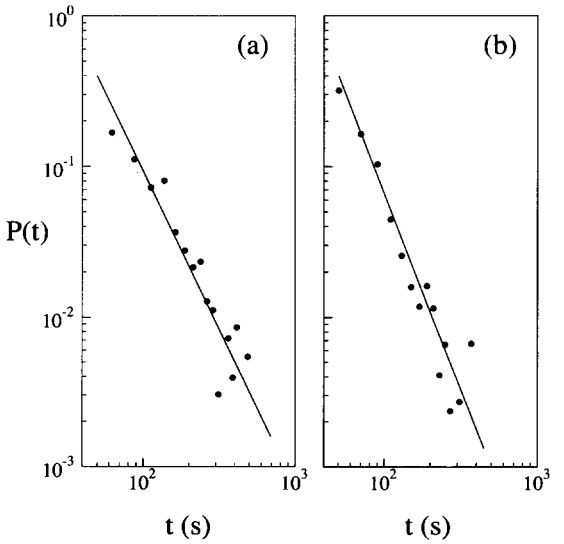

Fig. 16. (a) Sticking time and (b) flight time probability distribution functions for particles in the chaotic flow. The distribution functions are described by power laws with decay exponents $\nu = 2.1 \pm 0.3$ and $\mu = 2.6 \pm 0.3$, respectively.

6.4. Turbulent flow: no flights

The large Reynolds number and the absence of azimuthal jets leads to a behavior in the turbulent regime that contrasts markedly with that in the laminar and chaotic regimes. Tracers in the turbulent flow wander erratically, and there are no well-defined flights (which are dependent on jet regions) or sticking events: compare plots of trajectories in the turbulent flow, Figs. 17a, b, with those for the periodic flow, Figs. 6a–d, and compare plots of azimuthal displacement $\theta(t)$ in Fig. 17c with Fig. 7 and Fig. 13.

A scatter plot of $\theta(t)$, Fig. 18, shows a much more uniform spreading of an ensemble of particles than in the time-periodic case (Fig. 8) and the chaotic case (Fig. 14). The average angular deviations are much smaller for a given time than for the periodic and chaotic flows, due to the absence of long-range flights. The slope γ of a log–log plot of the variance $\sigma^2(t)$ (Fig. 19) drops steadily from 2 and appears to approach the value expected for normal diffusion ($\gamma = 1$) at long times; however, we cannot follow particles for long enough times to determine the asymptotic behavior.

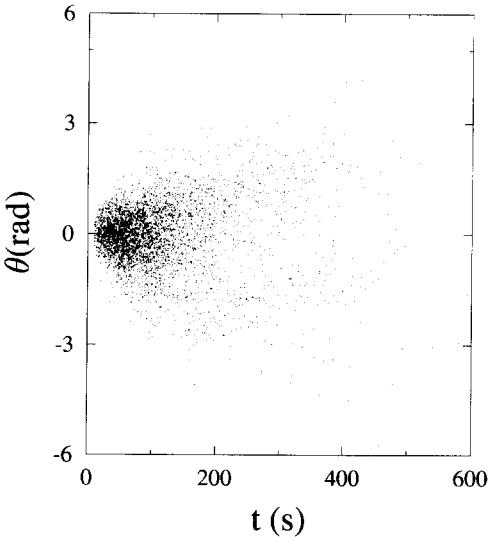

Fig. 18. Scatter plot showing the azimuthal positions of an ensemble of particles at discrete times, for the turbulent flow.

There are no flights or sticking events in the turbulent flow, but by treating the trajectories as random walks, we can define a step as the time between two successive extrema in $\theta(t)$. We find that the probability distribution function is exponential, $P(t) = A\,e^{-t/\tau}$, with $A = 0.158$ and $\tau = 15.2$ s (see Fig. 20), in contrast to the power law

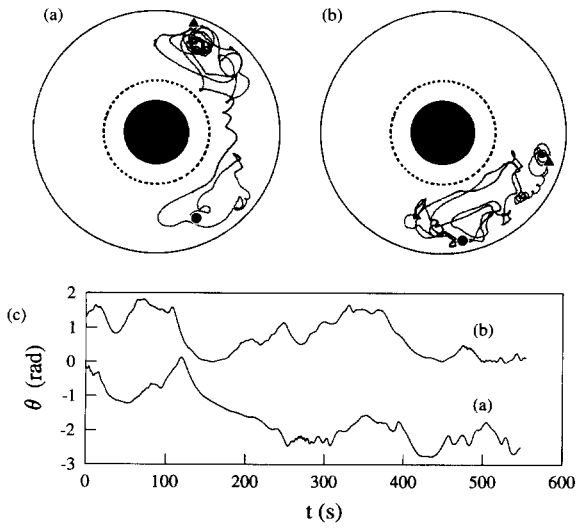

Fig. 17. (a) and (b) Tracer particle trajectories in the turbulent flow, viewed in the annulus reference frame. (c) The azimuthal displacement for the particles in (a) and (b).

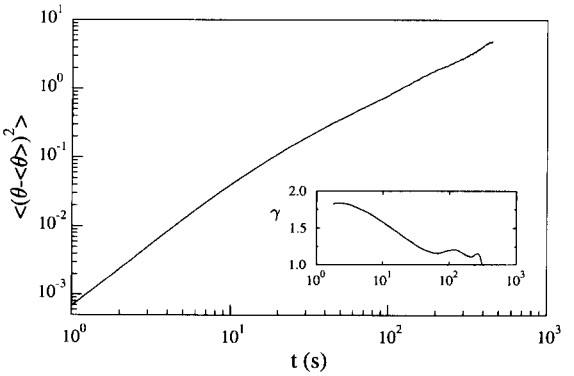

Fig. 19. Variance of the azimuthal displacement of about 1300 tracer particle trajectories in a turbulent flow. The slope in the inset decreases monotonically toward unity and has no plateau, in contrast to the cases for superdiffusion; compare Fig. 9 and Fig. 15.

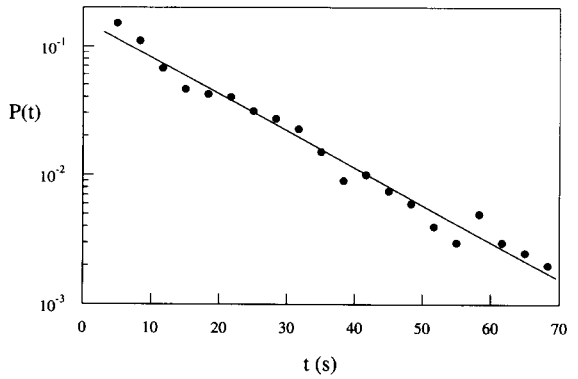

Fig. 20. Probability distribution for azimuthal displacement in the turbulent flow. The distribution is exponential with a decay time of 15.2 s.

PDFs observed for flights in the time-periodic and chaotic regimes.

7. Discussion

The data from the four regimes are summarized in Table 1. The results from the time-periodic and chaotic regimes can be used to test theoretical predictions relating flight/sticking time statistics to superdiffusive transport. Eq. (2), which assumes that Lévy flights dominate the behavior, is in good agreement with our results for both of these regimes. Eq. (3), which relates the variance exponent to the power law exponents for both the sticking and flight PDFs, is consistent with the observations for the time-periodic regime, given the uncertainty in our exponent values. However, for the chaotic regime, the latter theory predicts an increase in γ to a value greater than 2; although the experimental uncertainties are larger in this regime, the data appear to be inconsistent with the prediction.

Table 1
Exponents ν and μ characterizing the power law decay of probability distribution functions for the sticking and flight times, respectively, and the exponent γ for the power-law time dependence of the variance of the azimuthal displacement.

Flow regime (co-rotating frame)	ν	μ	γ
Time-independent	N/A[a]	N/A[a]	2
Time-periodic	1.6 ± 0.3	2.3 ± 0.2	1.65 ± 0.15
Chaotic	2.1 ± 0.3	2.6 ± 0.3	1.55 ± 0.25
Weakly turbulent	N/A[a]	N/A[a]	~1

[a] N/A = not applicable.

Several theories have analyzed power law sticking behavior in model systems. There is no universal agreement about the decay exponent, or even if the exponent should be universal. Exponents ranging from $\nu = 0.7$–3.8 have been predicted for different systems [18,20–25,36,37]. In one numerical study, values of ν ranged from 0.7 to 2.8 for a single system, depending on the parameters of the model [37]. Our experimental values of ν (1.6 for time-periodic and 2.1 for chaotic regimes) are consistent with this picture of a non-universal exponent.

In summary, by tracking large numbers of tracer particles in a two-dimensional flow, we are able to obtain direct experimental evidence of Lévy flights and anomalous diffusion. The motion of tracer particles is dominated by clearly distinguished sticking and flight events that alternate irregularly in time. The probability distribution functions for both sticking and flight events are described by power laws for the periodic and chaotic flows examined; the exponent values depend on the parameters of the flow. The exponent for the variance of the displacement for the periodic and chaotic flows lies in the range $1 < \gamma < 2$, i.e., the motion is superdiffusive. Future work will involve studies of subdiffusion ($\gamma < 1$) in experiments with alternating forcing.

Acknowledgements

We thank D. del-Castillo-Negrete, P. Morrison, M. Pervez, M. Shlesinger, J. Urbach and G. Zaslavsky for helpful comments. This research is supported by the Office of Naval Research Grant No. N00014-89-J-1495.

References

[1] B.D. Hughes, M.F. Shlesinger and E.W. Montroll, Random walks with self-similar clusters, Proc. Natl. Acad. Sci. USA 78 (1981) 3287–3291.

[2] E.W. Montroll and M.F. Shlesinger, in: Nonequilibrium Phenomena II: From Stochastics to Hydrodynamics Studies in Statistical Mechanics, vol. II, eds. J.L. Lebowitz and E.W. Montroll (North-Holland, Amsterdam, 1984) pp. 1–119.

[3] M.F. Shlesinger, G.M. Zaslavsky and J. Klafter, Strange kinetics, Nature 363 (1993) 31–37.

[4] W. Young, A. Pumir and Y. Pomeau, Anomalous diffusion of tracers in conductive rolls, Phys. Fluids A 1 (1989) 462–469;
O. Cardoso and P. Tabeling, Anomalous diffusion in a linear system of vortices, Eur. J. Mech. B/Fluids 8 (1989) 459–470.

[5] T. Geisel, J. Nierwetberg and A. Zacherl, Accelerated diffusion in Josephson junctions and related chaotic systems, Phys. Rev. Lett. 54 (1985) 616–619;
T. Geisel, A. Zacherl and G. Radons, Generic $1/f$ noise in chaotic Hamiltonian dynamics, Phys. Rev. Lett. 59 (1987) 2503–2506; Chaotic diffusion and $1/f$-noise of particles in two-dimensional solids, Z. Phys. B (1988) 117–127.

[6] J. Klafter, A. Blumen and M.F. Shlesinger, Stochastic pathway to anomalous diffusion, Phys. Rev. A 35 (1987) 3081–3085.

[7] X.-J. Wang, Dynamical sporadicity and anomalous diffusion in the Lévy motion, Phys. Rev. A 45 (1992) 8407–8417.

[8] G.M. Zaslavsky and M.K. Tippett, Connection between recurrence-time statistics and anomalous transport, Phys. Rev. Lett. 67 (1991) 3251–3254.

[9] V.V. Afanasiev, R.Z. Sagdeev and G.M. Zaslavsky, Chaotic jets with multifractal space–time random walk, Chaos 1 (1991) 143–159.

[10] T.H. Solomon, E.R. Weeks and H.L. Swinney, Observation of anomalous diffusion and Lévy flights in a two-dimensional rotating flow, Phys. Rev. Lett. 71 (1993) 3975–3978.

[11] J. Sommeria, S.D. Meyers and H.L. Swinney, Experiments on vortices and Rossby waves in eastward and westward jets, in: Nonlinear Topics in Ocean Physics, ed. A. Osborne (North-Holland, Amsterdam, 1991) pp. 227–269.

[12] R.P. Behringer, S.D. Meyers and H.L. Swinney, Chaos and mixing in a geostrophic flow, Phys. Fluids A 3 (1991) 1243–1249.

[13] T.H. Solomon, W.J. Holloway and H.L. Swinney, Shear flow instabilities and Rossby waves in barotropic flow in a rotating annulus, Phys. Fluids A 5 (1993) 1971–1982.

[14] M.S. Pervez and T.H. Solomon, Long-term tracking of neutrally buoyant tracer particles in two-dimensional fluid flows, Exp. Fluids, in press.

[15] H. Aref, Stirring by chaotic advection, J. Fluid Mech. 143 (1984) 1–21.

[16] T.H. Solomon and J.P. Gollub, Passive transport in steady Rayleigh–Bénard convection, Phys. Fluids 31 (1988) 1372–1379.

[17] J.M. Ottino, Mixing, chaotic advection and turbulence, Ann. Rev. Fluid Mech. 22 (1990) 207–253.

[18] J.D. Meiss and E. Ott, Markov-tree model of intrinsic transport in Hamiltonian systems, Phys. Rev. Lett. 55 (1985) 2741–2744.

[19] G.M. Zaslavsky, D. Stevens and H. Weitzner, Self-similar transport in incomplete chaos, Phys. Rev. E 48 (1993) 1683–1694.

[20] J.D. Meiss and E. Ott, Markov tree model of transport in area-preserving maps, Physica D 20 (1986) 387–402.

[21] C.F.F. Karney, Long-time correlations in the stochastic regime, Physica D 8 (1983) 360–380.

[22] B.V. Chirikov and D.L. Shepelyansky, Correlation properties of dynamical chaos in Hamiltonian systems, Physica D 13 (1984) 395–400.

[23] Y.-C. Lai, R. Blümel, E. Ott and C. Grebogi, Quantum manifestations of chaotic scattering, Phys. Rev. Lett. 68 (1992) 3491–3494.

[24] J.B. Weiss and E. Knobloch, Mass transport and mixing by modulated traveling waves, Phys. Rev. A 40 (1989) 2579–2589.

[25] C. Jung, T. Tel and E. Ziemniak, Application of scattering chaos to particle transport in a hydrodynamic flow, Chaos 3 (1993) 555–568.

[26] G.M. Zaslavsky, to be published.

[27] T.H. Solomon and J.P. Gollub, Chaotic particle transport in time-dependent Rayleigh–Bénard convection, Phys. Rev. A 38 (1988) 6280–6286.

[28] R. Ramshankar and J.P. Gollub, Transport by capillary waves. Part II: Scalar dispersion and structure of the concentration field, Phys. Fluids A 3 (1991) 1344–1350.

[29] A.R. Osborne, A.D. Kirwan, A. Provenzale and L. Bergamasco, Fractal drifter trajectories in the Kuroshio extension, Tellus 41A (1989) 416–435.

[30] M.G. Brown and K.B. Smith, Ocean stirring and chaotic low-order dynamics, Phys. Fluids A 3 (1991) 1186–1192.

[31] A. Ott, J.P. Bouchaud, D. Langevin and W. Urbach, Anomalous diffusion in "living polymers": A genuine Lévy flight?, Phys. Rev. Lett. 65 (1990) 2201–2204.

[32] J. Pedlosky, Geophysical Fluid Dynamics (second Ed.) (Springer, New York, 1987).

[33] S. Elghobashi and G.C. Truesdell, Direct simulation of particle dispersion in a decaying isotropic turbulence, J. Fluid Mech. 242 (1992) 655–700.

[34] I. Mezic and S. Wiggins, Birkhoff's ergodic theorem and statistical properties of chaotic dynamical systems, to be published.

[35] D. del-Castillo-Negrete and P.J. Morrison, Chaotic transport by Rossby waves in shear flow, Phys. Fluids A 5 (1993) 948–965.

[36] C.F. Hillermeier, R. Blümel and U. Smilansky, Ionization of H. Rydberg atoms: Fractals and power-law decay, Phys. Rev. A 45 (1992) 3486–3502.

[37] Y.-C. Lai, M. Ding, C. Grebogi and R. Blümel, Algebraic decay and fluctuations of the decay exponent in Hamiltonian systems, Phys. Rev. A 46 (1992) 4661–4669.